Surface & Coatings Technology 465 (2023) 129570

Contents lists available at ScienceDirect

Surface & Coatings Technology

journal homepage: www.elsevier.com/locate/surfcoat

Mechanical properties optimization of Cr_3C_2-NiCr coatings produced by compact plasma spray process

Felice Rubino [a,*], David Merino [a], Alessia Teresa Silvestri [b], Claudio Munez [a], Pedro Poza [a]

[a] DIMME – Durability and Mechanical Integrity of Structural Materials, Universidad Rey Juan Carlos. Escuela Superior de Ciencias Experimentales y Tecnología. C/ Tulipán s.n., 28933 Móstoles, Madrid, Spain
[b] Department of Chemical, Materials and Production Engineering, University Federico II of Naples, P. le Tecchio, 80, 80125 Naples, Italy

ARTICLE INFO

Keywords:
Thermal spray
Compact plasma spray
Chromium carbides
Design of experiments
Process optimization

ABSTRACT

Chromium carbides are widely used as functional coatings on steel structures in high-end applications, from energy to marine and aerospace sectors thanks to their corrosion and wear resistance at elevated temperatures. In the present work, a low-power compact plasma spray (CPS) equipment was used to deposit Cr_3C_2-based cermet coatings on carbon steel substrate. Design of experiment was applied to select and optimize the spraying parameters, namely current, stand-off distance, scanning speed, plasma gas rate and powder feeding rate. ANOVA analysis was conducted to estimate the effect of the spraying variables on morphology and mechanical properties of the coatings and evaluate the optimal spraying condition. Dense and compact coatings were fabricated by using the CPS. By optimizing the processing parameters, coating hardness equal to approximately 600 HV and average thickness ranging around 600 μm were obtained, while the adhesion strength was approximately equal to 14 MPa. Intermediate phases of Cr carbides were produced by the dissolution of the primary Cr_3C_2 induced by melting and re-solidification of the particles. The presence of weaker carbide phase, inter-lamellae different features and porosity also caused the scattered hardness values observed in the coatings.

1. Introduction

Surface engineering and manufacturing coating technologies have been developed and widely implemented to protect engineering products, such as turbine machinery elements, power generation units, components for aerospace, automobiles as well as oil and gas industry, against failure when working in corrosive or high temperature environments and extend their life span [1–4]. The predominant mechanisms leading to the degradation of these components are essentially wear, corrosion, erosion, and cavitation, which events can involve complex mechanical, chemical, and electrochemical interactions between the environment and materials [5]. Therefore, the coatings should be able to withstand the severe working conditions and possess high mechanical and thermal resistance, both in the case of static or dynamic loads, and chemical stability [6,7]. Among the multiple coating techniques developed in the last decades, such as physical (PVD) and chemical (CVD) vapor deposition, laser cladding, nitriding, the thermal spraying (TS) processes demonstrated to be the most suitable solution to overcome these limitations [8]. TS techniques, indeed, can deposit many types of materials, such as metals, ceramics, or their mixtures; the thickness of the coating can range from a few microns up to millimeters, making them suitable for several applications, and the deposited coatings achieve outstanding wear and corrosion resistance [9]. Among the several thermal spray processes, Plasma Spray has gained a solid interest from specialists and researchers thanks to its intriguing advantages, e.g., higher coating density and bond strength (which ranges from 30 MPa up to 70 MPa) due to the high particle velocity, higher deposition rate and temperature [1]. The accurate tuning of particle velocity, heating level, stand-off distance, and the other parameters allows to control and optimize the coating structure and the performance. Many contributions can be found in published literature discussing the influence of those variables on the hardness, microstructure, residual stresses, and bonding [1,10]. As far as the materials currently used as protective coating [1,6,7], chromium-based carbides are particularly interesting to be used in several applications. Cr_3C_2 based coatings, for example, provide outstanding tribological properties in harsh environments and severe operating conditions, like turbine blades or boilers [11]. Plasma sprayed chromium-carbide based coatings demonstrated high wear and corrosion resistance at elevated temperatures improving the operative life of the components. In addition, the formation of highly stable and hard

* Corresponding author.
E-mail address: felice.rubino@urjc.es (F. Rubino).

https://doi.org/10.1016/j.surfcoat.2023.129570
Received 8 February 2023; Received in revised form 17 March 2023; Accepted 22 April 2023
Available online 3 May 2023

chromium oxide phase during the deposition prevents the penetration of abrasive particles and protects the subsurface of the substrate from degradation [12–14].

Chromium carbides are usually coupled with a softer metallic phase to form cermet composite systems. Ni-Cr metallic alloys, in particular, are used to facilitate the deposition of carbides power and, at the same time, improve the toughness and the ductility of the coatings [15–17]. In addition, nickel-chromium binder improves erosion and corrosion resistance, thanks to the higher percentages of chromium in the coating [18–21]. However, Cr_3C_2-NiCr coatings are particularly sensitive to the deposition technique adopted and the selected spray parameters. Two aspects were pointed out as of outmost relevance and directly connected to the manufacturing route: the residual porosity inside the coating and the carbide dissolution [22,23]. Porosity influences the corrosion and erosion resistance of the coating/substrate system. High levels of porosity, indeed, favors the propagation of the corrosion medium through the coating and aggravates the galvanic corrosion mechanism, leading to the weakening of the bonding interface; furthermore, it reduces the coating hardness, making the coating prone to the eroded by incident objects [23]. Cr_3C_2-based coatings can experience dissolution of the carbide during the thermal spraying. Degradation of carbide content and decarburization usually lead to a formation of cracks network after the deposition and to a reduced wear resistance. Key parameters, such as plasma gas type, gas flow rate, power, etc., affect the carbide dissolution within the metallic binder [24]. Despite the wide documentation available on the use of chromium carbide-based cermet coatings for wear and corrosion protection, other potential usages for TS coatings have not yet considered, it is the case of the solar power applications, on which very few studies have focused, and the published literature is still scarce [8]. TS coatings, indeed, do not have competitive optical performances in terms of absorptance and selectivity of optical properties if compared to the consolidated methodologies, such as chemical deposition or wet chemistry. The complex microstructure, the surface roughness, the deposition defects, and other not-fully understood aspects influence the interaction of light with the coating in an unpredictable way. In addition, the coatings must possess the required structural and chemical integrity to guarantee the wanted working life [8,25]. Finally, the dimensions of the components of a solar power plant to be coated obstacle the diffusion in solar power field of conventional TS processes, which require controlled environmental conditions and large equipment with several ancillary tools. Solar receivers, heat exchangers or storage tanks cannot be easily disassembled for the coating deposition or maintenance operations. In this context, investigating the influence of the deposition process on optical properties and identifying novel strategies and approaches for in-situ manufacturing and post-deposition treatment of TS coatings are of paramount importance.

In the present work, the feasibility of compact plasma spray (CPS) process to deposit chromium carbide-based cermet coatings is studied. This low-power plasma spray equipment was proposed instead of conventional high-power one, since it is able to be used for in-situ manufacturing of coatings on large components, like those working in solar power plants. Chromium carbide-Ni20Cr powders system, commercially known as WOKA 7102, was considered in the present work to be deposited by using CPS on steel substrates. Indeed, the constituents of WOKA 7102 have good properties in term of solar absorptance. Nickel and chromium, for instance, at the operating temperature of the solar absorbers tend to form stable oxides (also known as black nickel and black chromium) with an average value of absorptance well above 0.9 [26]. Chromium carbide also has good intrinsic optical properties [27,28], however the deposition of coatings consisting of only carbide by processes different from the vacuum techniques is still challenging [29]. WOKA powders systems are usually deposited by Atmospheric Plasma Spray and High Velocity Oxi-Fuel (HVOF) [1,30] and the cermet coatings produced by adopting the recommended procedure have excellent properties [31]. However, as mentioned, the conventional HVOF equipment it is not suitable for solar absorbers in concentrating solar power plant. Therefore, the manufacturing of WOKA 7102-based coatings by low-power plasma spray has been investigated in the present work. Obviously, the recommendations provided by the manufacturers of the powders and the equipment are not suitable for the conditions explored here and the information about the processing parameters are extremely scarce, resulting in coatings that do not have the standard microstructure and properties. Therefore, investigation on the optimal deposition conditions and on the influence of processing parameters is crucial.

The effects of five process parameters, namely velocity of plasma gun, stand-off distance, current, plasma gas rate, and powder feed rate, on the system responses were investigated. The outputs considered were the thickness of the coating, the adhesion strength with the substrate and the Vickers hardness. The surface roughness was also considered, but only as a control property and, hence, not included in the optimization procedure of the deposition process.

2. Experimental procedure

The substrate material selected for the present study was T22 carbon steel. Its chemical composition is reported in Table 1, as provided by the vendor. The T22 substrate was provided in the form of 3 m long bars with a rectangular cross section of 40 × 5 mm^2. The bars were sliced by band sand machine into 40 mm × 40 mm × 5 mm rectangular coupons. Prior the deposition, the coupons were grit blasted using white Al_2O_3 particles at a pressure of 4 bar to eliminate grease or surface oxides and modify the surface roughness.

The substrates were, then, coated by using compact plasma spray process with commercially available Cr_3C_2-20($Ni_{20}Cr$) powders. The powders were provided by Oerlikon Metco under the commercial name of Woka 7102 [31]. Differently from other commercial systems consisting in mechanical mixture of hard and soft phases, Woka 7102 is composed by chromium carbide particles coated by Ni20Cr alloy powders (80/20 wt%) (see Fig. 1). The resulting coating presents a complex structure consisting of a hard phase mixed with the softer matrix (the metallic constituents) that acts as a binder, facilitating the adhesion of ceramic with the substrate and the cohesion between the particles and, thus, the formation of a compact and stable coating. The average diameter of particles is between 10 and 45 μm, which is particularly suitable for the CPS system, which is characterized by short dwelling time of particles inside the plasma stream and, thus, reduced heating up.

The CPS Sulzer Metco equipment was used to produce the cermet coatings on the T22 substrate. The present paper aims to optimize the processing parameters to obtain a sound coating, however, it is important to mention that not all the parameters can be varied, and some of them are fixed. It is due to the fact the CPS equipment was designed as portable and to be used on-site.

The type of gas usable with the gun is argon and the pressure is determined by the CPS manufacturer. The powder injector is located at the exit of the nozzle and perpendicular to the plasma stream. Therefore, only the parameters that can be modified during the service of the CPS were investigated. Those parameters are: i) scanning velocity of the plasma gun, ii) stand-off distance between the substrate surface and the exit of the nozzle and, iii) current, iv) flow rate of the plasma gas, and v) powder feeding rate. The parameters selected showed a significant influence on the properties of the manufactured coatings [25,26]. Other parameters, namely the rate of the carrier gas and of the shroud gas, were not modified during the present experimentation despite the CSP equipment allows to change them. It is because the value of those two parameters is strongly connected to the above-mentioned conditions and especially to the plasma gas rate. Arbitrary variation in those parameters can lead to instability of the plasma and incorrect working of the CPS equipment. The flow rate of carrier and shroud gases was chosen according to the practical experiences of the authors. Design of experiment (DoE) approach was used to investigate the influence of the five variables on the microstructural and mechanical properties of the Cr_3C_2-20

Table 1
Chemical composition of T22 substrate and Woka 7102 powders.

Substrate and powders	Chemical composition (wt%)							
	Fe	C	Cr	Ni	Mn	Si	S	Mo
T22	Bal.	0.11	1.93	–	0.43	0.27	0.011	0.92
Woka 7102	<0.5	9.6–10.8	Bal.	13.5–18.5	–	–	–	–

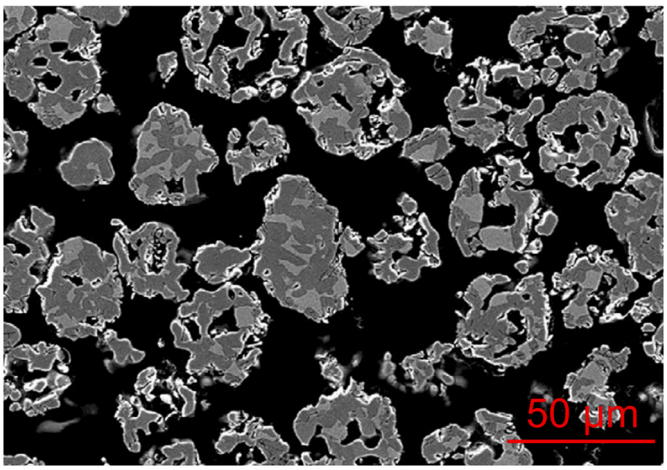

Fig. 1. SEM images of Cr_3C_2-NiCr powders at different magnifications. (Courtesy from Oerlikon Metco [31].)

($Ni_{20}Cr$) cermet coatings. Initially, two levels were selected for screening purpose for each parameter. The choice was dictated by the number of parameters considered and by the necessity of keeping moderate the number of runs. To avoid mislead conclusions on the effects of the selected parameters from the experiments, due to the high variability of the responses, the values of the low (−1) and high (+1) levels in the design of experiment were set as distant as possible according to the capability of the CSP gun, technological limits, and previous experiences of the authors. It allowed to achieve a reasonable estimation of the true effect of the factors. Table 2 summarizes the process parameters and the values corresponding to the two levels.

Because the first DOE was intended for screening experiments, a fractional factorial design, 2^{k-1} with k = 5, was designed to reduce furtherly the number of runs. In previous work of some of the authors [25] it was observed that, for what concerns the compact plasma spray, main effects and two-factors interactions were the most significant, while the high order interactions can be neglected. It supports the choice of a fractional design, which is enough to estimate the 5 main effects and the 10 two-factor interactions. Further process conditions, called star or axial points, were also added to the factorial runs in the design of experiments to estimate potential quadratic effects of the variables on the response variables. The center point of the DOE, which is replicated six times, and ten axial runs were, therefore, selected defining a central composite design. The values of the process variables for the axial runs were selected according to the formula $\alpha = (n_f)^{1/4}$, where n_f is the number of the fractional factorial runs to build a rotatable central composite design [32].

Table 3 shows the factorial plan with 32 experimental runs, which were conducted randomly to avoid any systematic error. Four features of the coatings were investigated in the screening experiments, namely thickness and surface roughness of the coatings, which can be referred as morphological responses, adherence and hardness that correspond to the mechanical responses of the coatings. As previously mentioned, the surface roughness was taken as control property.

The next step of the experimentation was to apply a different 2-levels central composite design centered on the processing region, where the maximum thickness, the adherence, and the hardness were observed. Only two parameters, namely the plasma gas rate and the gun velocity, were selected in the second optimization step. Tables 4 and 5 report the

Table 2
Process parameters of CPS system and respective levels adopted in 2^{5-1} fractional factorial plan for Woka 7102.

Process parameters		Level	
		−	+
A	Gun velocity (m/s)	0.015	0.02
B	Stand-off-distance (mm)	120	180
C	Current (A)	48	56
D	Plasma gas rate (NLPM)	0.82	1.21
E	Feeder (FMR)	40	60
Other deposition parameters			
Carrier gas rate (NLPM)		0.25	
Shroud gas rate (NLPM)		3.68	

NLPM: normalized liter per minute of argon.
FMR: flow-meter readings.

Table 3
Two levels fractional factorial (2^{k-1}) design with k = 5 processing factors showing the levels for WOKA 7102 (center points and star points are shaded).

Run	Factor				
	Gun Velocity (m/s)	Stand-off distance (mm)	Current (A)	Plasma (NLPM)	Powder Feeder (g/min)
B001	0.0175	150	52	1.02	4.96
B002	0.0175	150	60	1.02	4.96
B003	0.02	180	48	1.21	3.64
B004	0.0175	150	52	1.02	4.96
B005	0.02	120	56	0.82	6.39
B006	0.0175	150	52	1.43	4.96
B007	0.02	180	56	0.82	3.64
B008	0.0175	150	52	1.02	4.96
B009	0.0175	150	52	1.02	4.96
B010	0.02	180	48	0.82	6.39
B011	0.015	180	48	1.21	6.39
B012	0.02	180	56	1.21	6.39
B013	0.0175	90	52	1.02	4.96
B014	0.0125	150	52	1.02	4.96
B015	0.015	120	48	0.82	6.39
B016	0.015	180	56	0.82	6.39
B017	0.0175	150	52	0.61	4.96
B018	0.0175	210	52	1.02	4.96
B019	0.0175	150	44	1.02	4.96
B020	0.015	120	48	1.21	3.64
B021	0.015	120	56	1.21	6.39
B022	0.015	120	56	0.82	3.64
B023	0.0175	150	52	1.02	2.44
B024	0.0175	150	52	1.02	7.92
B025	0.02	120	48	0.82	3.64
B026	0.015	180	48	0.82	3.64
B027	0.0175	150	52	1.02	4.96
B028	0.0175	150	52	1.02	4.96
B029	0.0225	150	52	1.02	4.96
B030	0.02	120	56	1.21	3.64
B031	0.015	180	56	1.21	3.64
B032	0.02	120	48	1.21	6.39

Table 4
Parameters of CPS system and respective levels adopted for the second 2^2 factorial plan.

Process parameters		Level	
		−	+
A	Gun velocity (m/s)	0.017	0.02
B	Plasma gas rate (NLPM)	1.07	1.37
Other deposition parameters			
Stand-off-distance (mm)		110	
Current (A)		56	
Feeder (FMR)		60	
Carrier gas rate (NLPM)		0.25	
Shroud gas rate (NLPM)		3.68	

NLPM: normalized liter per minute of argon.
FMR: flow-meter readings.

Table 5
Two levels full factorial (2^k) design with k = 2 processing factors, center points with two replication and four star points (center points and star points are shaded).

Run	Factor	
	Gun Velocity (m/s)	Plasma (NLPM)
C001	0.0185	1.21
C002	0.02	1.37
C003	0.0185	1.21
C004	0.02	1.07
C005	0.017	1.07
C006	0.017	1.37
C007	0.0185	1.43
C008	0.0185	1.02
C009	0.016	1.21
C010	0.021	1.21

value of the processing parameters of the new DoE and summarize the spraying conditions. The choice of the fixed and variable parameters for the 2nd experimental campaign as well as the selection of the values for the processing parameters were based on the result from the 1st round of experiments and aiming to optimize the three features studied. The 2nd experimental campaign individuated the optimal values for the remaining parameters in order to maximize the adherence and hardness, while the thickness was kept as control factor.

Coating thickness and hardness were evaluated on the cross section of the coated samples. The samples were cut using an IsoMet 5000 abrasive cutting machine along the parallel and transversal directions to the gun movement direction and hot mounted in phenolic epoxy resin (by using the Buheler SimpliMet 1000). The samples were then polished by using a grinding/polishing machining (model EcoMet 250 from Buheler) according to the following procedure: grinding phases with P120 grit paper until plane and P320, P600, and P1200 grit paper, polishing with 9 μm, 3 μm and 1 μm diamond slurry.

The thickness of the coatings was estimated by using optical microscopy (Model BA310Met from MOTIC). At least, thirty measures were acquired for the coating thickness from each sample from micrographs. The micrographs were captured in random locations of the cross section at different magnifications. The Vickers microhardness was measured by using a Buehler 2100 microhardness tester on the cross-sections of polished samples, adopting 100 g as load and of 15 s as dwell time. The microhardness of the coatings may be affected by the presence of the hard (Cr_3C_2) and the metal (Ni-Cr) phases and the registered values may depend on the specific location where the indentations have been made. Therefore, four profiles of indentations, 100 μm distant from each other, were done along the through-thickness directions. Each profile consisted of a maximum of 10 indentations; consecutive indentations were kept distant three times the bigger indentation diagonal to avoid the influence of the stress field generated by the neighboring indentations. The value of coating microhardness here reported was the average of the four profiles.

Selected polished samples were also analyzed through scanning electron microscopy (SEM), Hitachi S-3400N SEM, provided with energy dispersive X-ray spectroscopy (EDX) probe to assess the distribution of the hard and the metal phases and the presence of the secondary phases resulting from the reaction of the carbide with metallic alloys during the plasma deposition. The arithmetic average roughness (Ra) of the deposited coatings was measured with the Mitutoyo SJ-301 portable surface roughness tester. The measurements were taken according to the ISO 4287-1997 standard, adopting a sampling length of 4 mm. Eight profiles were acquired for each sample. X-ray diffractograms (XRD) were obtained from the plain-view surface of the coating. The coatings were previously sand grit to remove the external surface. A X'pert Pro diffractometer (PANalytical) were used, which employs Cu-Kα radiation. The angular range scanned was 10 to 115°, with a step size of 0.04 and 1 s per step.

The adherence strength was measured following the ASTM D4541 [33]. The pull-off tests were conducted by using a portable testing machine (DeFelsko PosiTest AT-A20). A dolly, having 10 mm diameter contact surface, was glued onto the coating surface using Araldite® 2011-A/B (from Huntsman) adhesive and then cured in an oven at 160 °C for 1 h, to achieve the maximum strength of the adhesive (rated 50 MPa). After the pull-off test, the optical microscope was used to determine whether there was residue of coating on the substrate. For each experiment, the average was computed from five replications.

3. Results and discussion

3.1. Analysis of the effects of processing parameters

The measured data of morphological and mechanical properties of the coatings are summarized in Fig. 2.

As expected, coating thickness, adhesion strength, hardness, and roughness are influenced by the process parameters adopted: the response of the system, indeed, noticeably varies when the level of the factors is changed during the experimental campaign. Coating thickness showed a strong dependence on the spraying parameters, as visible in the wide scattering in the measured values along the experimental configurations. The thickness, indeed, was found to range from a maximum of 600 μm to a minimum below 50 μm. For practical application of the plasma sprayed coating, a thickness below 100 μm is considered unacceptable, because it leads to poor cohesion and weak consolidation with the substrate, as confirmed by the adherence and hardness tests. Sample B003, for instance, attained the lowest value of thickness of approximately 16 μm, which made impossible to collect reliable measures of adherence and hardness (that are registered as zeros). Other configurations, having values of thickness below 100 μm, showed a null value of adherence due to the impossibility of performing proper measurements on too small and fragmented coatings. Vickers hardness does not show the same correlation with the thickness of the adherence, and except for the mentioned B003 case. The other low-thickness configurations showed average hardness compatible with the remaining test cases, where the variations have to be ascribed to the different combinations of parameters. Figs. 3 and 4 report the main effects of each factor and the Pareto charts with the standardized effects for the coating properties.

According to the estimated effect of the factors on the coating thickness (see Table 6), the projection distance is the one that presents the greater influence, followed by the powder feeding rate. Current and gun velocity, show a remarkable effect despite their contributions are not as relevant as the former parameters (see Fig. 4), while the plasma

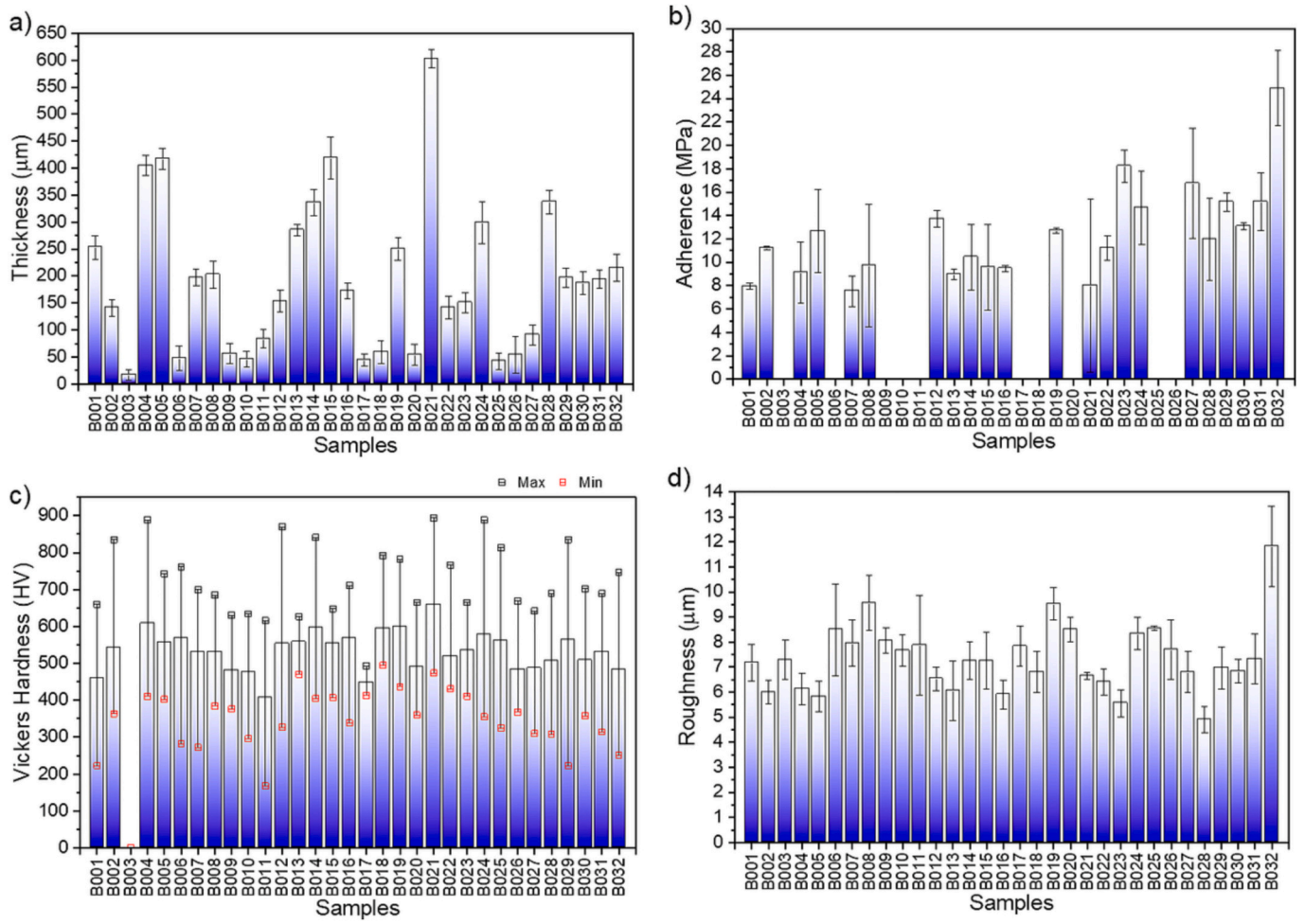

Fig. 2. Bar graphs of the measured coating properties of the samples from the first experimental run: a) Coating thickness; b) adherence; c) Vickers hardness; d) surface roughness (Ra).

has a negligible effect, contributing only for the 5 % to the global output. Its interaction with the other parameters, despite being higher than the main effect, can also be neglected with respect to the other parameters. The second order effect of plasma flow rate (D * D bar in Fig. 4a), on the other hand, is at the same level of gun velocity and current, pointing out a quadratic trend of the thickness with plasma gas rate (visible in Fig. 3d). The variation of plasma gas rate from 0.8 to 1.21 NLPM, indeed, caused an overall increment in the thickness of only 5 % (see Fig. 3d), however, at the 1.0 NLMP the average thickness increased of almost 25 %. The quadratic effect is also visible in hardness and roughness, despite to a lesser extent. In the case of coating adherence, only the linear analysis was conducted, but the similarity with the other mechanical property suggests that this trend could be confirmed.

High deviation was registered in the Vickers hardness of each sprayed sample, which can be ascribed to the heterogeneity of the composite coatings. The microstructure consists, indeed, of a mixture of harder carbide particles and the softer Ni-based matrix together with weaker zones at the interlamellar regions or due to lack of cohesion between the splats, which result in point-to-point variation of hardness within the same coating.

The average microhardness value was found to be around 600 HV, with peaks of 900 HV [19]. The values observed here are lower than that of coatings produced by conventional atmospheric plasma spray, which is around 1000 HV, this could be due to the lower spraying energy levels of the CPS [21]. Current, stand-off distance and powder feed rate were the most influential factors for the hardness, followed by the gun velocity slightly below the significance threshold and the plasma gas rate showing having half the influence of other factors (see Fig. 4 and Table 6). Plasma alone has a limited effect, as observed in the other properties, however its interaction with the other variables is relevant being the relative standardized effect above the level of significance (see Fig. 4). Hardness and thickness share a similar behavior with the processing variables: decrease of stand-off distance or gun velocity and increase in current or powder feed rate led to an increment of these properties. Furthermore, like the coating thickness, hardness showed quadratic behavior with plasma gas rate. Current directly affects the temperature and the travel speed of sprayed particles. Therefore, higher current promotes the melting of particles and their flow upon the substrate surface, forming well bonded lamellae and a more compact and dense coating. Relative motion between the plasma torch and the substrate is critical to produce a consistent and uniform coating: reducing the speed or the torch-to-substrate distance allows the particles to retain their velocity at the impact with the substrate resulting in highly flattened and compacted splats. Lowering the travel speed at constant powder feed rate, or vice-versa, causes the amount of particles projected onto the substrate to increase, favoring the build-up of a thicker and denser coating.

In the case of the adhesion strength, only the first order effect analysis was conducted, since some samples showing null values due to the impossibility of conducting proper measurements. Poor deposition conditions, having thicknesses below 100 μm, are associated with zero or very low adherence. Improper heating of particles or not sufficient kinetic energy can be the reason of a limited deformation of the particles at the impact, resulting in a weak interlocking of splats and poor

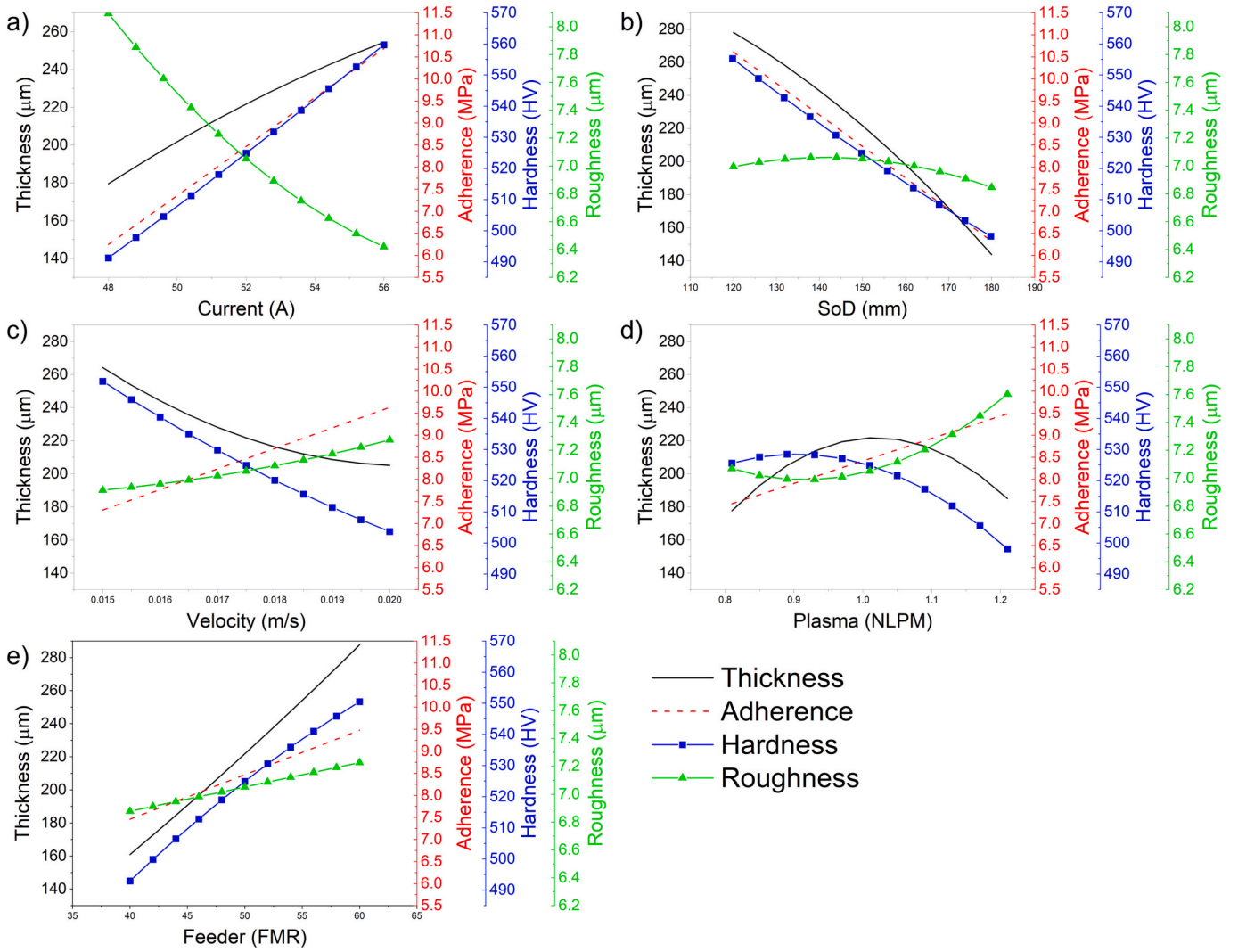

Fig. 3. Main effect plots of the processing parameters on coating responses: a) current; b) SoD; c) velocity; d) plasma; e) feeder.

interparticle cohesion and adhesion with the substrate. Too thick coatings also are characterized by lower adhesion with the substrate. Thick coating, indeed, exerts considerable shear stress on the substrate leading to the formation of residual stresses within the material and weakening the adhesion strength. Thickness ranging from 200 to 300 µm is the optimal conditions, which achieved the highest adherence within the present experimentation [25]. From the analysis, it is possible to preliminarily deduce that increasing the current and decreasing the projection distance allow maximizing the coating adhesion, while only a secondary control of powder feeder, gun velocity and plasma gas rate is needed due to their lower influence. However, it is worth to note the standardized effects of all parameters fall below the level of significance ($\alpha \approx 5$ %), therefore particular attention has to be paid in deriving these conclusions.

The average roughness, Ra, of the coatings (showed in Fig. 2d) significantly vary between the samples pointing out a relationship with the spraying parameters [11]. The flattening degree of the particles significantly influencing the roughness and can be correlated to temperature and impact velocity, and in such a way with the volume fraction of chromium carbide within the NiCr matrix [11]. It suggests that higher current should lead to lower average roughness. The factor effect analysis pointed out that current is the most influential among the parameters, with an average effect that is almost three times the one of the second parameters. Current is also predominant with respect to the factors' interaction (see Figs. 3 and 4). Therefore, the minimization of roughness can be pursued by reducing only the current according to the wanted goal and the final application of the coating. For the present application, aiming to obtain a coating with good mechanical properties and integrity, the priority has been done to the optimization of the other properties, while the roughness has been considered as control output.

By observing the results of the analysis of the first experimental campaign, some guideline can be drawn. Stand-off distance (B) has a limited influence on the adhesion, while keeps a close relationship with the coating thickness and the hardness. SoD values lower than those suggested by the manufacturer of the CPS system (which indicates a distance not below 135 mm for powders similar to WOKA) are recommended to maximize the mechanical properties of the coating. A value around 120 mm or lower can be adopted as long as it keeps the torch at an acceptable distance from the substrate. The SoD for the 2nd round was selected as low as possible in order to maximize the mechanical properties of the coatings. The adopted value of 110 mm was a trade-off between the mechanical properties and the risk of overheating of the substrate and delamination of the coating due to the excessive proximity of the gun with substrate. The model predicts that an optimal operating point can be found at high current, but it may cause that the power absorbed by the equipment overcomes the limits of 2.5 kW. Therefore, a limited regulation can be done on the current and the optimum point needs to be set at 56 A. The powder feed rate has low influence on the adhesion, while it has tangible effect on the thickness of the coating. Too high values are not suitable leading potentially to obstructions in the

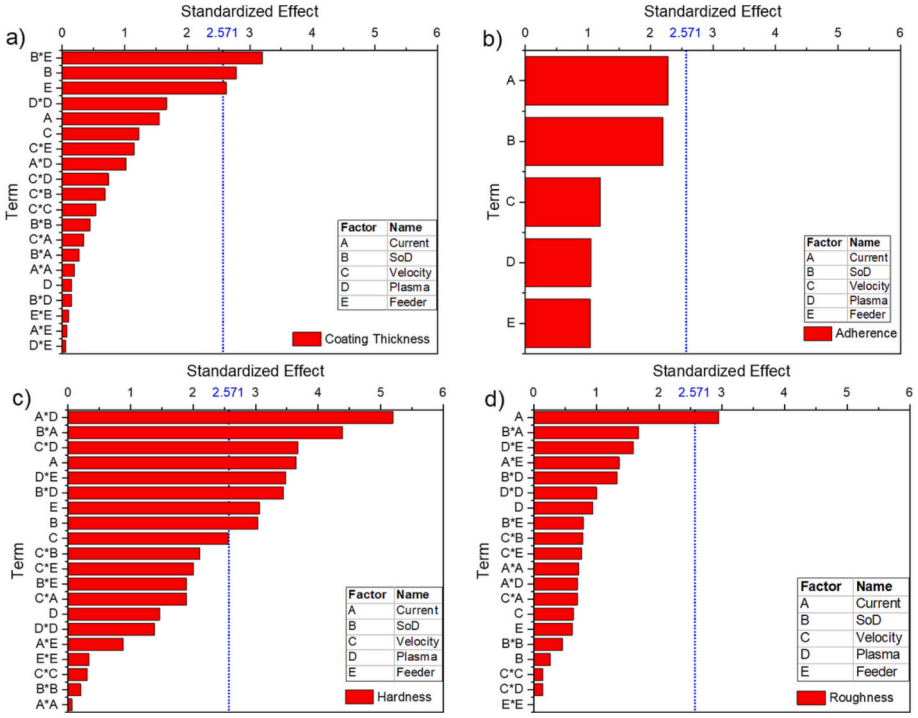

Fig. 4. Standardize effects of the processing parameters and their interactions on coating responses: a) Coating thickness; b) adherence; c) hardness; d) Ra roughness.

Table 6
Effect of the process parameters (gun velocity, stand-off-distance -SoD, plasma gas rate, current, powders feeder) on the coating properties.

	Thickness	Adherence	Hardness	Ra
Velocity	−59.1	2.16	−48.2	0.36
SoD	−134.4	−4.28	−57.1	−0.15
Current	74.9	4.47	68.5	−1.67
Plasma	7.6	2.04	−27.5	0.53
Feeder	126.7	2.00	57.5	0.35

powders' injector and instability in the plasma stream; therefore 6.4 g/min was set as the optimum point for this parameter. Stand-off distance, current, and powder feed rate were kept constant in the second round of experiments. Gun speed and Plasma gas rate presented peculiar trends for the coating properties: the former has a competitive effect for adhesion and thickness and the value has to be selected by balancing the two desiderata; the latter has a quadratic influence on hardness and thickness and a local optimal point needs to be searched. Therefore, optimal projection points are not easy to be found and a second round of tests focused on these two parameters was necessary. Gun speed and plasma gas flow rate have been redefined around the data obtained from the previous model limiting its high and low values; the two levels selected for the gun speed and plasma gas rate were 0.017 and 0.02 m/s, 1.05 and 1.35 NLPM, respectively (see Table 4). At this point, a 2^2 + star factorial experiment design was used to find out the curvature of the model and obtain the response surface for the parameters involved (see Table 5).

The results of the second round are reported in Fig. 5. Compared to the first round, the coating thickness achieved higher average increasing from 172 μm to 660 μm, while adherence and hardness registered only a slight change. The adhesion strength and hardness showed, also, a limited dispersion around their overall average of approximately 12.3 MPa and 560 HV, respectively. The second experimental window was designed around a narrower range of the variables and using optimized values for fixed parameters, leading to a lower variability (no >10 % and 40 % for hardness and adherence, respectively) with the processing conditions. Conversely, the coating thickness still showed a remarkable sensitivity to the spraying conditions. It can be ascribed to uncontrolled factors of the CPS equipment during the coating deposition, which are the power output and the voltage. In the CPS, indeed, only the current can be controlled, and the voltage value results when the plasma plume is formed. The voltage output also varies depending on the status of the consumable parts of the plasma gun, i.e., the electrode cathode, the nozzle and the anode. These components suffer the most wear during spraying. The wear alters their shape and reciprocal centering, affecting the voltage and, thus, the power output. This occurrence can be mitigated by planning maintenance actions to some extent, however some uncertainty on these factors is inevitable and unpredictable conditions can establish.

By analyzing the factors effect (Fig. 6 and Table 7), it is possible to observe changes in the main effect of velocity and plasma gas, as well as their interaction on the coating properties. Second order dependence also became more significant, especially for the thickness. Observing the coating thickness, indeed, the plasma gas rate showed higher influence in the first and second-order effects than that observed in the 1st round, while only a slight reduction has been observed for the velocity. The main and interaction effects on adhesion strength and hardness, on the other hand, maintained almost the same values of the main effects. It is important to note that the main effect of velocity on thickness and hardness changed sign in the 2nd round of experiments. It is visible by observing their trends reported in Fig. 6a. Potential changes in the behavior of the coating responses are expected, considering that the two rounds of experiments were conducted in different ranges of the processing parameters with three out of five kept constant, and interaction effects between fixed and variable parameters are not negligible as visible in Fig. 4. In addition, it is worth noting that the overall variation of thickness and hardness when velocity changes from level −1 to level +1 is approximately the 6 %.

The effect of the selected plasma variables on the adhesion, thickness, and hardness of the coating can be better estimated from the second quadratic order response. Response surfaces were constructed to predict the optimal parameters (Fig. 7). The contour charts of these surfaces help in predicting the coating properties in any region of the

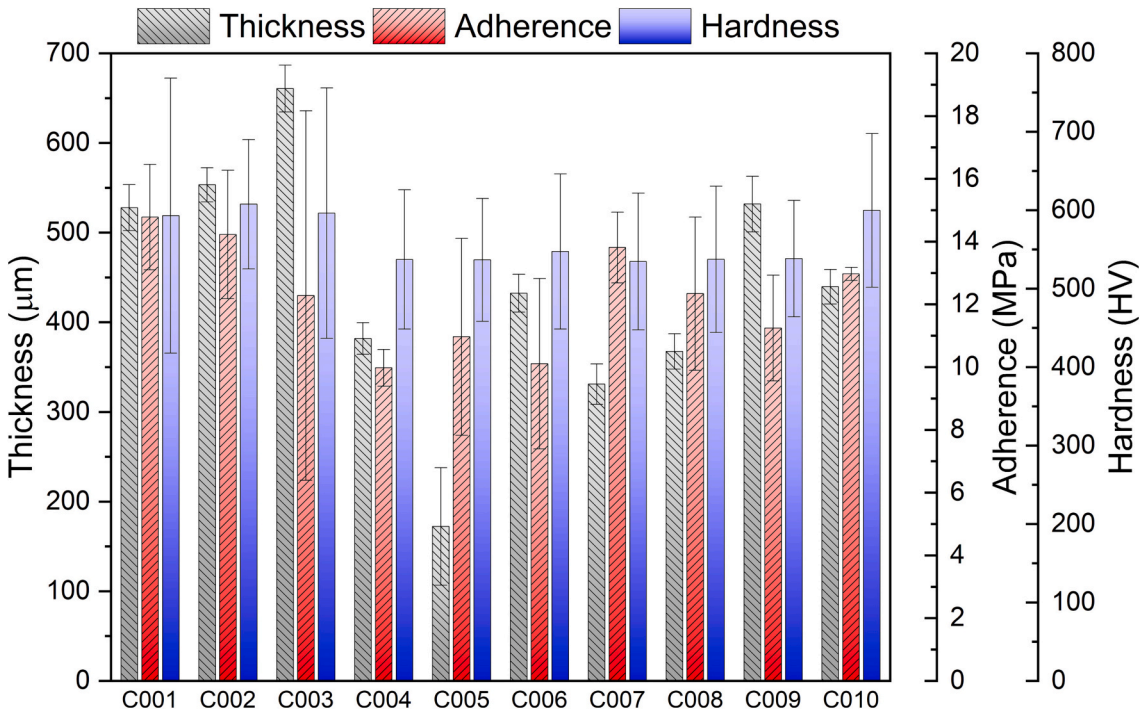

Fig. 5. Measured coating thickness, adherence and Vickers hardness of the samples from the second experimental round.

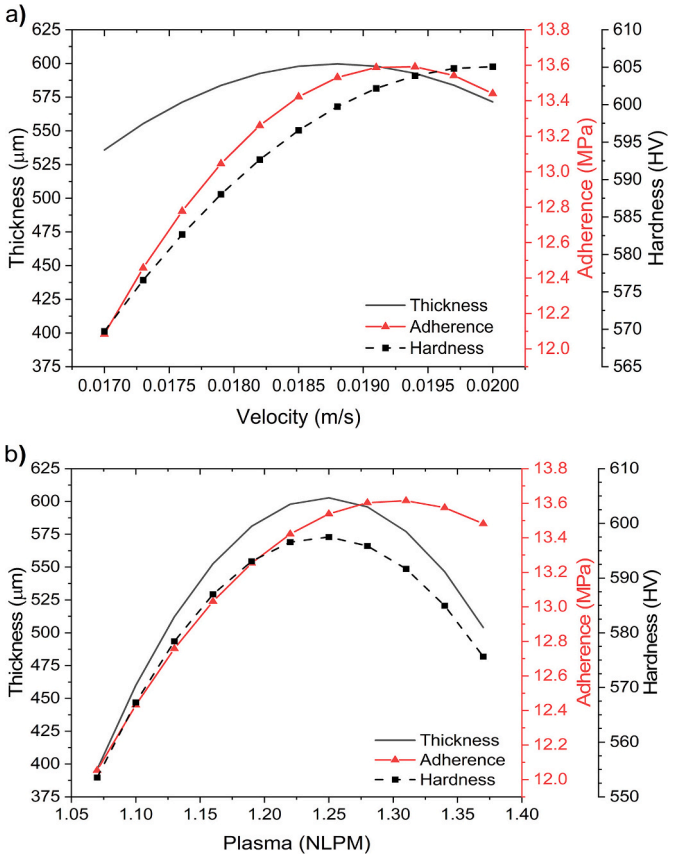

Fig. 6. Main effect plots of the processing parameters on coating responses: a) Velocity; b) plasma.

Table 7
Mean, quadratic and interaction effect of gun velocity and plasma gas rate on the coating properties.

	Thickness (µm)	Adherence (MPa)	Hardness
Velocity	35.6	1.36	35.3
Plasma	108.2	1.43	22.1
Velocity * velocity	−88.58	−1.32	−18.3
Plasma * plasma	−295.9	−1.31	−63.9
Velocity * plasma	−35.7	2.57	29.6

experimental domain.

The concentric ellipses observed in the thickness contour chart (Fig. 7a) point out a region of high thickness approximately at the central values of velocity and plasma.

The response surface model for the case of adhesion (Fig. 7b) has a hyperbolic geometry (or a half saddle), which shows a relative maximum in the right upper corner region corresponding to a gun velocity value of 0.02 m/s and a plasma value of 1.37 NLPM. The combination of these parameters has a positive effect on adhesion; therefore, they can be considered the projection optima in the experimental domain. The same can be inferred for the Vickers hardness. In this case, the highest hardness is achievable by maximizing the gun speed and by choosing a value of plasma gas close to 1.3 NLPM. Aiming to maximize the mechanical properties of Cr_3C_2-NiCr coating the confirming experiments were conducted selecting for the gun speed and the plasma gas rate values close to the upper right region, i.e., 0.021 m/s and 1.43 NLPM, respectively. It should lead to a lower value of thickness: the predicted values should fall in the range between 490 and 530 µm. The reduced thickness is not an issue, considering thermal sprayed coatings are prone to form intense residual stress fields, which are strongly dependent on the deposited material thickness, resulting in a weak bond and an easier in-service failure. Confirming experiments are used to verify the accuracy of the adhesion, thickness and hardness prediction developed for Cr_3C_2-20NiCr cermet coatings with respect to the selected parameters within the experimental domain. Four deposition tests with the aforementioned parameters were conducted. Table 8 shows the measurements of thickness, adherence, and hardness tests on the four

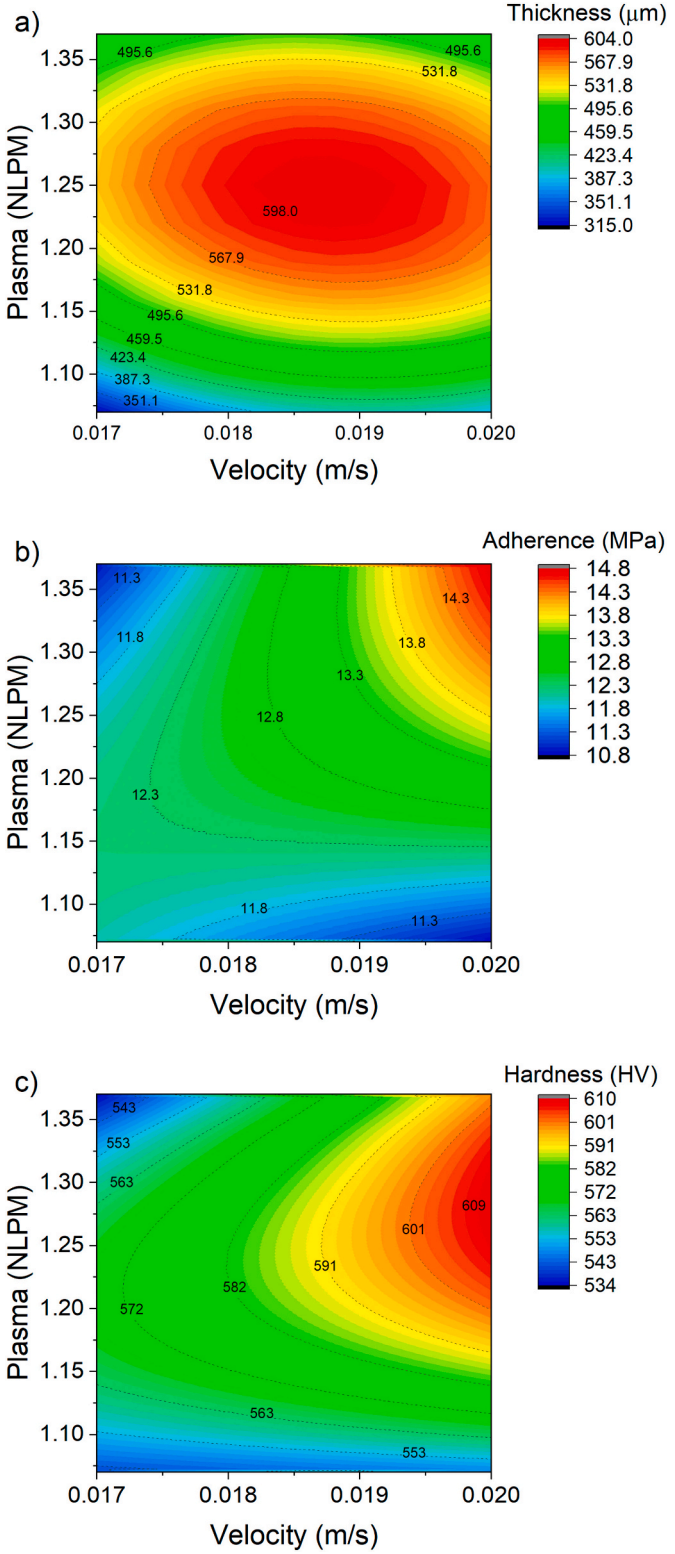

Fig. 7. Contours of response surfaces estimated for (a) adherence, (b) coating thickness and (c) hardness: plasma gas rate vs. gun velocity.

Table 8
Results from confirming experiments compared to the predicted values.

	Thickness (μm)	Adherence (MPa)	Hardness (HV)
Experiment	618.7 ± 30.1	13.4 ± 3.2	593.2 ± 24.2
Predicted	372.5	13.2	547.0

coatings and the predicted values from the model.

In the case of thickness, a significant deviation from the values obtained in the spraying tests of approximately 200 μm with respect to the prediction was observed. While, for adherence and hardness the models returned values closer to the experiments with a very limited discrepancy. The larger deviation between predicted and experimental values of the thickness can be ascribed to the fact that the second order regression model can be overfitting and have too many terms. The model was, indeed, enough good in fitting the experimental data but not reliable in predicting the new observations [32]. New tests may be beneficial to build a more reliable model for the coating thickness, however, since the first goal of the present work was to optimize the mechanical properties of the coatings and their predictions with current models were enough good, no further investigations were conducted. The thickness was, then, considered as control factor, as it reached the minimum expected value of 100 μm.

3.2. Coating microstructure

During the plasma spraying, the particles were heated up and accelerated towards the substrate. After the impact, the partially melted particles deform, taking the characteristic shape of splats and resolidify to form the coating. It essentially consists of layers of these splats overlapping each other due to the subsequent impact of molten or semi-molten particles onto the substrate and stacking one above another until the required thickness is obtained [34].

Typical coating microstructure consists of the melted and un-melted primary particles together with debris that unavoidably remain entrapped within the coating, derived by the in-flight oxidation at high temperature of the finer particles. Subsequent passages of plasma torch consolidate the particles inside the structure of the coating. The final deposited coating contains porosity, primary particles (molten splats and globular un-melted ones), oxides, debris, and fine peripheral particles, as visible in Fig. 8. In the present case, the metallic binder completely melts due to the higher temperature of the plasma and deforms at the impact with the substrate, forming very flattened splats. The metal phase covers the ceramic particles facilitating the adhesion on the substrate and the cohesion between the carbides, and fills the gaps between the harder particles promoting the building-up of the coating and the reduction of the porosity. However, the high melting point carbides caused the presence of unavoidable un-melted hard particles within the coating: small size carbide particles fragmented during the impact in smaller shreds, which distributed almost uniformly inside the soft metallic matrix, while bigger particles retained their original shape (see Fig. 8). The coating shows also a microstructure dominated by extensive crack network feature mainly localized in the inter-splat regions. Formation of porosities can be ascribed first to the specific deposition conditions used: lower particles velocities, typical of APS deposition with subsonic nozzle or due to the low power plasma spray, are commonly associated with the formation of crack network features as dominant porosity [22]. In addition, the presence of the shroud gas, surrounding the plasma jet, prevented a more extensive oxidation, but caused the cooling down of the largest sprayed particles resulting in a higher concentration of un-melted or partially melted splats. Residual stresses arising from the mismatching between the partially melted particles and the molten Ni-binder due to the different thermal expansion coefficients can cause the formation of shrinkage cracks at the boundaries of the phases. Cracks and lower inter-splat cohesion (highlighted by the clearly discernible lamellar structure in Fig. 8) are addressed as the cause premature spallation of the coating under erosive action [34]. Second, smaller pores can be induced by the presence of gas dissolved inside the molten particles, which remains entrapped during the deposition of the splats and leaks after the solidification of the coating, as well as by the pull-out of the weakly adhered splats during the metallographic preparation [22].

The microstructure of the Cr_3C_2-NiCr coating consists of darker

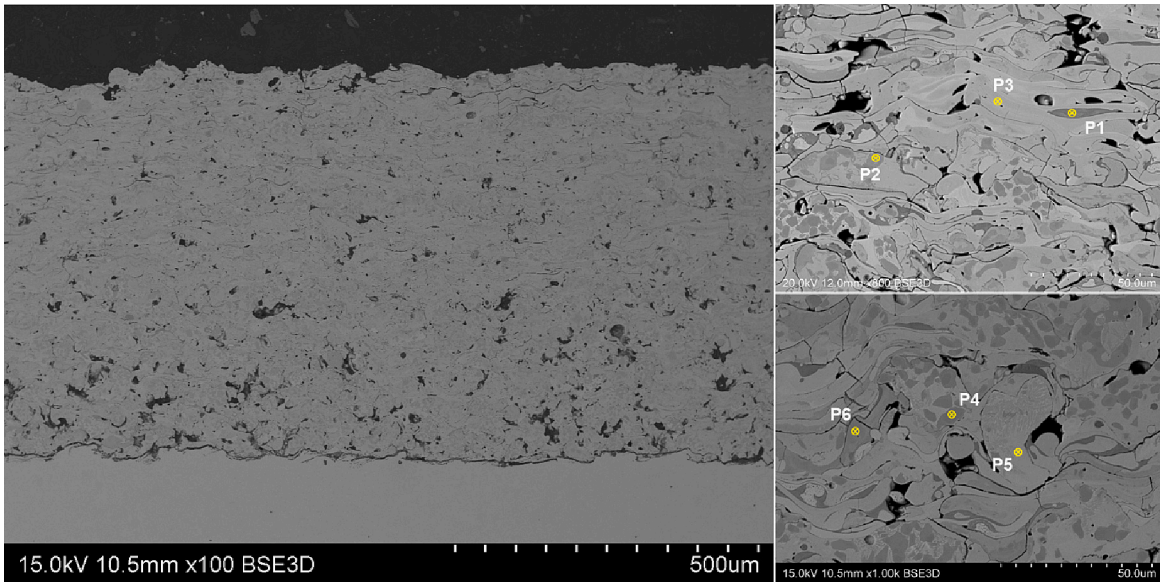

Fig. 8. BSE images of the sprayed WOKA coating at different magnifications.

regions composed by chromium, carbon, and oxygen, which represent the primary carbide, with a negligible or no presence of nickel. Brighter areas indicate regions where the carbide dissolved into the nickel matrix. Table 9 reports the results of the EDX analysis on the different phases observed within the coating. The EDX analysis revealed the presence of chromium and nickel inside the coating confirming the composite nature of the coating made by Cr_3C_2, nickel and chromium. Darkest areas (P1 spot in Fig. 8) are associated to phase rich in oxygen and chromium with a limited and almost negligible amount of carbon and nickel. The detected percentages of elements are close to the stoichiometric composition the Cr_2O_3. Dark gray particles (spots P2, P4 and P6 in Fig. 8), more evenly distributed within the coating, are characterized by a pronounced presence of chromium and carbon, while no significant traces of oxygen or nickel were detected, suggesting that these particles can be derived from the pristine chromium carbide in the Woka 7102. They may represent the different chromium carbide solid phases, i.e., Cr_7C_3 and $Cr_{23}C_6$. The gray areas are Ni-rich zones (P3 and P5 in Fig. 8). The Ni-rich regions showed a large gray scale distribution suggesting a variable amount of carbides dissolved into the NiCr phase during the deposition [12]. The whiter flattened zone is the Ni-based metallic binder, while the gray zones represent supersaturated Ni/Cr/C solid solution derived by the dissolution of carbide. The black regions represent the entrapped voids or pores [12]. Surely, the EDX results here reported can give only qualitative information about the different chromium carbides and oxides within the metallic matrix of the thermal sprayed coatings. The black scattered SEM imaging and EDX analysis, indeed, allowed to distinguish the carbides from oxides but was not able to separate the different species of chromium carbides and chromium oxides owing to their close composition range.

Fig. 9 shows the XRD spectrum of the CPS-WOKA 7102 coating. The XRD pattern indicates clear peaks of the two chromium carbides Cr_7C_3 and $Cr_{23}C_6$ phases along with Ni alloy phase. The peaks are broader than those observable in the pristine material due to the dissolution of the carbides and the formation of amorphous phase as consequence of fast cooling [18]. The presence of chromium oxide Cr_2O_3 was not clearly recognized probably due to the limited oxidation occurred during the spraying with inert carrier gas, while larger amount of the oxide phase was detected in coatings deposited with different techniques [34]. No traces of Cr_3C_2 phase were detected in the plasma sprayed coating. It confirms the hypothesis about the complete dissolution of the pristine carbide during the deposition.

The elemental maps of Cr, C and Ni (see Fig. 10) indicate the distribution of secondary carbide within the binder regions. Limited oxygen traces were also detected in the microstructure of the coating as result of in-flight oxidation. Some bright globular particles are visible: they could be the bigger pristine Woka particles that are un-melted during the deposition and retain approximately their original size (approximately 30 μm).

EDX and XRD analyses point out the formation of intermediate phase of chromium carbides (Fig. 8 and Table 9). Several studies showed that Cr_7C_3 and $Cr_{23}C_6$ stable solid phases form together with chromium oxides during the deposition by plasma spray technique as consequence of decarburization of the pristine Cr_3C_2 and oxidation phenomena according to the suggested sequence [34–36]: $Cr_3C_2 \rightarrow Cr_7C_3 \rightarrow Cr_{23}C_6 \rightarrow [Cr] \rightarrow Cr_2O_3$. The mechanisms behind the formation of the stable phase of chromium carbide during the thermal spraying are still object of study but some hypotheses can be formulated. The Cr_7C_3 phase tends to form around the Cr_3C_2 particles (see P1 in Fig. 8) suggesting that the Cr_7C_3 particles formation resulted from the decarburization of Cr_3C_2, and they are characterized by a higher percentage of carbon than the $Cr_{23}C_6$

Table 9
Elemental composition estimated from EDX analysis at distinct locations of the coating.

Element	P1		P2		P3		P4		P5		P6	
	wt%	at.%	wt%	at.%	wt%	at.%	wt%	at.%	wt%	at.%	wt%	at.%
C	1.2	3.1	4.7	19.2	3.0	12.8	7.0	23.8	4.4	16.7	5.9	20.5
O	28.1	55.3	–	–	–	–	1.7	4.3	1.0	2.9	2.0	5.2
Cr	64.0	38.8	81.5	77.0	69.9	69.9	90.6	71.4	62.0	54.4	90.1	72.3
Ni	4.4	2.4	3.3	2.8	18.5	16.4	0.8	0.5	32.0	24.9	1.2	0.9
Si	0.4	0.5	–	–	–	–	–	–	0.6	1.0	0.8	1.2
W	–	–	3.6	1.0	3.4	1.0	–	–	–	–	–	–

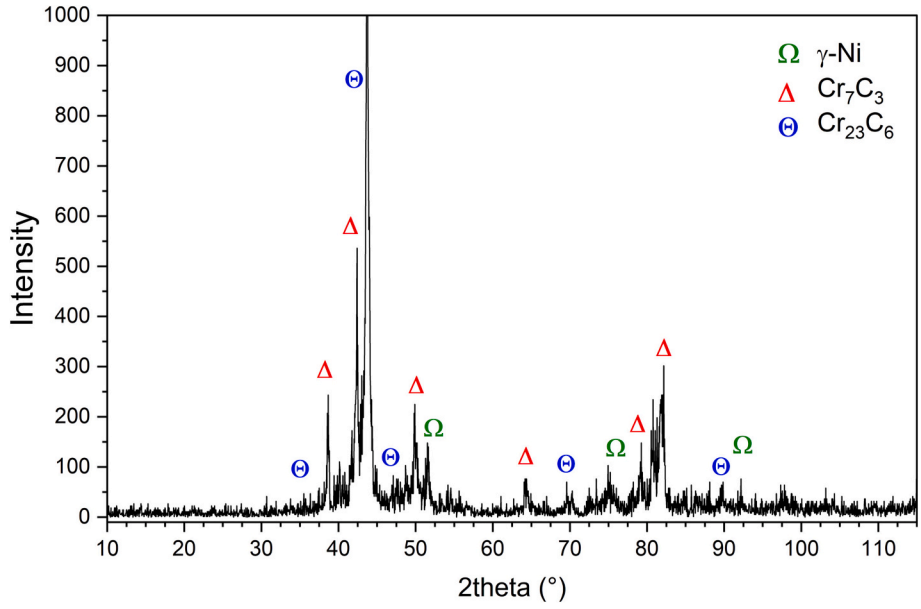

Fig. 9. XRD spectra of CPS-WOKA 7102 coating.

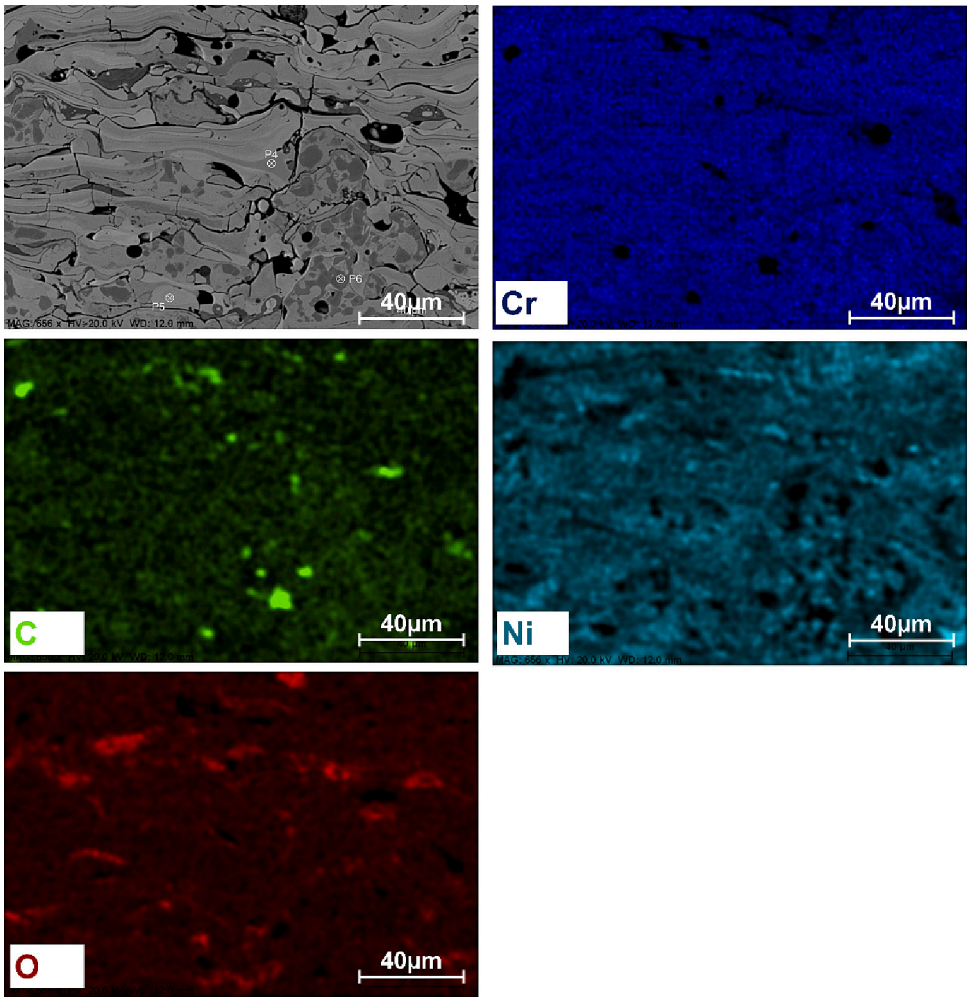

Fig. 10. Elemental maps of WOKA7102 coating.

phase [37]. The decomposition of the Cr_3C_2 is also confirmed by the lower values of hardness measured. Cr_3C_2 is, indeed, characterize by a hardness of approximately 1300 HV, while the average CPS coating hardness is around 600 HV [38]. During the spraying the Cr_3C_2 phase from the powders transforms into the liquid phase and graphite [37], however after the deposition due to the rapid solidification the material is not able to reform the pristine carbide phase and Cr_7C_3 plus graphite phases are produced. These phases have much smaller hardness and, together with the microcracks at the lamellae boundaries, contribute to the low values detected in the chromium carbide cermet coating [38].

On the other hand, $Cr_{23}C_6$ particles are smaller than those of Cr_7C_3 phase and are dispersed in the Ni-rich matrix mainly. It indicates that this phase forms mainly by precipitation mechanism during the deposition [35]. Some studies suggested that during the quenching or a very rapid solidification the Cr-C system tends to form the metastable Cr_3C phase, which subsequently transform in the $Cr_{23}C_6$. This transformation was usually observed in the case of annealing of chromium carbide compound at 700 °C [37] and in annealing of HVOF Cr_3C_2-NiCr coatings at 400 °C. Therefore, the presence of small particles of this phase in the CPS coating indicates that the precipitation mechanism continues during the cooling process of the deposited splats. The high temperature of the plasma spraying and the low level of oxygen in the process, if compared to other TS processes, like HVOF, limited the oxidation of the particles (which could be beneficial for the erosion resistance of the coating since the hardness of the Cr_2O_3 is around 3000 HV [38]) and favor the dissolution of Cr_3C_2 as primary mechanism [34]. Only few traces of chromium oxide were, indeed, found in the CPS coating, which can be ascribed more to the oxidation of the NiCr alloy matrix than that of the carbide particles [35]. In addition, while the mentioned TS process is characterized by a very high particle velocity during the deposition, which favor the retention of the original carbide, in the plasma sprayed coatings the lower velocities also promote the dissolution of the pristine carbide and the EDX analysis did not detect remarkable traces of Cr_3C_2. The observed blurry gray areas surrounding the irregular carbides indicate the occurrence of carbide diffusion within the Ni-Cr binder. Dissolved elements of Cr-C remain entrapped inside the rapidly solidifying NiCr binder, however, the amount of Cr-C elements exceeds the solid solubility in Ni and tends to form the supersaturated Ni/Cr/C solid solution [12]. Furthermore, the rapid solidification (cooling rates around 10^6 and 10^8 K/s are reported in thermal spray of Cr carbide-NiCr systems [35]) also can lead to the binder forming an amorphous phase.

4. Conclusions

Low-power plasma spray equipment was used to deposit Cr_3C_2-NiCr powders on steel substrate. The design of experiments approach has been adopted to assess the feasibility of the proposed technology to deposit the material and the role of the processing of thickness, hardness, adhesion strength and surface roughness of the coatings. From the analysis of the results of the experimental campaign, some conclusions can be drawn:

1. Compact plasma spray equipment was able to deposit chromium carbide-NiCr cermet coating. However, not all the processing conditions were suitable to manufacture a compact and dense coating. Low current or too fast deposition resulted in coatings having thicknesses below 100 μm, which were characterized by poor or null adhesion with the substrate.
2. Coating thickness was found to be mostly influenced by stand-off distance, powder feed rate and current; furthermore, the second order plasma flow rate has a remarkable influence. Hardness was mostly affected by the same factors, while for surface roughness only the current was above the significance threshold. No clear information could be derived for the adhesion strength during the first round of the experiment due to the excessive number of trials returning a null value.
3. The results of first round experimental campaign indicate the highest level of current and powder feed rate and the lowest level of stand-off distance as optimal configuration to maximize the thickness and the hardness of coatings. The results related to plasma gas rate and gun velocity didn't reveal optimal projection points. Surface roughness was excluded as system response and kept as controlling parameter. Therefore, based on optimized values of current, powder feed rate and stand-off distance, the second round of experiments was designed, focusing on the influence of plasma gas rate and gun scanning velocity.
4. The results of second round experimental campaign highlighted a pronounced quadratic trends with gun speed and plasma gas rate. The outcomes indicate the highest level of plasma gas rate and gun velocity as optimal configuration to maximize the mechanical properties, i.e. hardness and adhesion, while maintaining satisfactory thickness values.
5. 110 mm, 56 A, 6.4 g/min, 0.021 m/s, and 1.43 NLPM were selected for stand-off distance, current, feed rate, speed, and plasma gas rate, respectively as optimal spraying configuration. Predicted results for hardness and adhesion strength well matched the confirmatory experiment with an error minor than 8 % and 2 %, respectively. The model failed to predict the value of the coating thickness with an error of almost 70 %. It was probably due to the sensitivity of the thickness to the spraying conditions, therefore unpredictable fluctuations in the operating conditions led to significant variations in the outcomes and then, limited the effectiveness of the model in predicting new observation.
6. The deposited coatings showed a complex microstructure consisting of molten splats and partially melted particles surrounded by the Ni-Cr binder. Intermediate phases of CrC compound were also observed due to the dissolution of the primary Cr_3C_2 carbide induced by the melting and fast re-solidification of the particles. The presence of weaker carbide phase and of inter-lamellae porosity caused the lower and wide scattered hardness values observed in the coatings.

CRediT authorship contribution statement

Felice Rubino: Data curation, Formal analysis, Investigation, Methodology, Validation, Visualization, Writing – original draft, Writing – review & editing. **David Merino:** Data curation, Formal analysis, Investigation, Methodology, Validation, Writing – original draft, Writing – review & editing. **Alessia Silvestri:** Investigation, Writing – original draft, Writing – review & editing. **Claudio Munez:** Conceptualization, Funding acquisition, Methodology, Supervision, Writing – review & editing. **Pedro Poza:** Conceptualization, Funding acquisition, Methodology, Resources, Visualization, Writing – review & editing.

Declaration of competing interest

The authors declare that they have no known competing financial interests or personal relationships that could have appeared to influence the work reported in this paper.

Data availability

Data will be made available on request.

Acknowledgments

This project was supported by the European Union's Horizon 2020 - Research and Innovation Framework Programme under the H2020 Marie Skłodowska-Curie Actions grant agreement No. 754382. The authors also wish to thank "Comunidad de Madrid" and European

Structural Funds for their financial support to the ACES2030-CM project (S2018/EMT-4319). The authors also would like to acknowledge the financial support received from the Spanish government AEI under Grant No. PID2020-115508RB-C22 (A3M).

References

[1] A.R. Govande, A. Chandak, B.R. Sunil, R. Dumpala, Carbide-based thermal spray coatings: a review on performance characteristics and post-treatment, Int. J. Refract. Met. Hard Mater. 103 (2022), 105772, https://doi.org/10.1016/j.ijrmhm.2021.105772.

[2] P. Carlone, A. Astarita, F. Rubino, N. Pasquino, P. Aprea, Selective laser treatment on cold-sprayed titanium coatings: numerical modeling and experimental analysis, Metall. Mater. Trans. B 47 (2016) 3310–3317, https://doi.org/10.1007/s11663-016-0636-7.

[3] F. Rubino, V. Paradiso, A. Astarita, P. Carlone, A. Squillace, Advances in titanium on aluminium alloys cold spray coatings, in: Cold-Spray Coatings, Springer International Publishing, Cham, 2018, pp. 225–249, https://doi.org/10.1007/978-3-319-67183-3_7.

[4] F. Rubino, A. Astarita, P. Carlone, S. Genna, C. Leone, F.Memola Capece Minutolo, A. Squillace, Selective laser post-treatment on titanium cold spray coatings, Mater. Manuf. Process. 31 (2016) 1500–1506, https://doi.org/10.1080/10426914.2015.1037912.

[5] R.J.K. Wood, B.G. Mellor, M.L. Binfield, Sand erosion performance of detonation gun applied tungsten carbide/cobalt-chromium coatings, Wear 211 (1997) 70–83, https://doi.org/10.1016/S0043-1648(97)00071-9.

[6] A. Meghwal, S. Matthews, H. Howse, C.C. Berndt, A.S.M. Ang, Steam and air oxidation behaviour of thermal spray chromium carbide-based composite coatings, Int. J. Refract. Met. Hard Mater. 111 (2023), 106088, https://doi.org/10.1016/j.ijrmhm.2022.106088.

[7] L.R. Umashanker, T.P. Bharathesh, B.R. B, S. R, Transitional wear of plasma spray Cr2O3 and Cr3C2 coatings deposited on low carbon steel, Int. J. Emerg. Sci. Eng. 10 (2022) 1–7, https://doi.org/10.35940/ijese.D2524.0310422.

[8] F. Rubino, P. Poza, G. Pasquino, P. Carlone, Thermal spray processes in concentrating solar power technology, Metals (Basel) 11 (2021) 1377, https://doi.org/10.3390/met11091377.

[9] M. Cadenas, R. Vijande, H.J. Montes, J.M. Sierra, Wear behaviour of laser cladded and plasma sprayed WC Co coatings, Wear 212 (1997) 244–253, https://doi.org/10.1016/S0043-1648(97)00127-0.

[10] F. Rubino, A. Astarita, P. Carlone, Thermo-mechanical finite element modeling of the laser treatment of titanium cold-sprayed coatings, Coatings 8 (2018) 219, https://doi.org/10.3390/coatings8060219.

[11] M.H. Staia, T. Valente, C. Bartuli, D.B. Lewis, C.P. Constable, A. Roman, J. Lesage, D. Chicot, G. Mesmacque, Part II: tribological performance of Cr3C2-25% NiCr reactive plasma sprayed coatings deposited at different pressures, Surf. Coat. Technol. 146–147 (2001) 563–570, https://doi.org/10.1016/S0257-8972(01)01438-4.

[12] Y. Zhang, K. Chong, Q. Liu, Y. Bai, Z. Zhang, D. Wu, Y. Zou, High-temperature tribological behavior of thermally-treated supersonic plasma sprayed Cr3C2-NiCr coatings, Int. J. Refract. Met. Hard Mater. 95 (2021), 105456, https://doi.org/10.1016/J.IJRMHM.2020.105456.

[13] B.K. Rakhadilov, Y. Tyurin, D. Kakimzhanov, D. Baizhan, O. Kolisnichenko, L. Zhurerova, Deposition of duplex Cr3C2-NiCr coatings on steel using a combined technique of gas detonation spraying and pulse-plasma treatment, High Temp. Mater. Processes 25 (2021) 25–37, https://doi.org/10.1615/HighTempMatProc.2021040480.

[14] A.R. Mayer, H.D.C. Fals, L.A. Lourençato, A.G.M. Pukasiewicz, in: Evaluation of the Chromium Carbide Deposited by HVOF for High Pressure Die Casting Molds, 2022, pp. 884–892, https://doi.org/10.31399/asm.cp.itsc2022p0884.

[15] M. Manjunatha, R.S. Kulkarni, M. Krishna, Investigation of HVOF Thermal sprayed Cr3C2-NiCr cermet carbide coatings on erosive performance of AISI 316 molybdenum steel, Procedia Mater. Sci. 5 (2014) 622–629, https://doi.org/10.1016/J.MSPRO.2014.07.308.

[16] T. Varis, T. Suhonen, O. Calonius, J. Čuban, M. Pietola, Optimization of HVOF Cr3C2NiCr coating for increased fatigue performance, Surf. Coat. Technol. 305 (2016) 123–131, https://doi.org/10.1016/J.SURFCOAT.2016.08.012.

[17] V. Matikainen, H. Koivuluoto, P. Vuoristo, A study of Cr3C2-based HVOF- and HVAF-sprayed coatings: abrasion, dry particle erosion and cavitation erosion resistance, Wear 446–447 (2020), 203188, https://doi.org/10.1016/J.WEAR.2020.203188.

[18] J.K.N. Murthy, K. Satya Prasad, K. Gopinath, B. Venkataraman, Characterisation of HVOF sprayed Cr3C2-50(Ni20Cr) coating and the influence of binder properties on solid particle erosion behaviour, Surf. Coat. Technol. 204 (2010) 3975–3985, https://doi.org/10.1016/J.SURFCOAT.2010.04.069.

[19] N. Espallargas, J. Berget, J.M. Guilemany, A.V. Benedetti, P.H. Suegama, Cr3C2–NiCr and WC–Ni thermal spray coatings as alternatives to hard chromium for erosion–corrosion resistance, Surf. Coat. Technol. 202 (2008) 1405–1417, https://doi.org/10.1016/J.SURFCOAT.2007.06.048.

[20] L.A. Luiz, J. de Andrade, C.M. Pesqueira, I.B. de A.F. Siqueira, G.B. Sucharski, M. J. de Sousa, Corrosion behavior and galvanic corrosion resistance of WC and Cr3C2 cermet coatings in Madeira River Water, J. Therm. Spray Technol. 30 (2021) 205–221, https://doi.org/10.1007/S11666-021-01152-8/FIGURES/11.

[21] A.H. Yaghtin, E. Salahinejad, A. Khosravifard, A. Araghi, A. Akhbarizadeh, Corrosive wear behavior of chromium carbide coatings deposited by air plasma spraying, Ceram. Int. 41 (2015) 7916–7920, https://doi.org/10.1016/J.CERAMINT.2015.02.131.

[22] S. Matthews, Carbide dissolution/carbon loss as a function of spray distance in unshrouded/shrouded plasma sprayed Cr3C2-NiCr coatings, J. Therm. Spray Technol. 24 (2015) 552–569, https://doi.org/10.1007/s11666-014-0210-2.

[23] H. Lu, J. Shang, X. Jia, Y. Li, F. Li, J. Li, Y. Nie, Erosion and corrosion behavior of shrouded plasma sprayed Cr3C2-NiCr coating, Surf. Coat. Technol. 388 (2020), 125534, https://doi.org/10.1016/J.SURFCOAT.2020.125534.

[24] S. Matthews, Development of high carbide dissolution/low carbon loss cr 3 C 2 –NiCr coatings by shrouded plasma spraying, Surf. Coat. Technol. 258 (2014) 886–900, https://doi.org/10.1016/j.surfcoat.2014.07.062.

[25] A. Rico, A. Salazar, M.E. Escobar, J. Rodriguez, P. Poza, Optimization of atmospheric low-power plasma spraying process parameters of Al2O3-50wt% Cr2O3 coatings, Surf. Coat. Technol. 354 (2018) 281–296, https://doi.org/10.1016/j.surfcoat.2018.09.032.

[26] D. Merino-Millan, C.J. Múnez, M.Á. Garrido-Maneiro, P. Poza, Alternative low-power plasma-sprayed inconel 625 coatings for thermal solar receivers: effects of high temperature exposure on adhesion and solar absorptivity, Sol. Energy Mater. Sol. Cells 245 (2022), 111839, https://doi.org/10.1016/j.solmat.2022.111839.

[27] G.L. Harding, Sputtered metal carbide solar-selective absorbing surfaces, J. Vac. Sci. Technol. 13 (1976) 1070–1072, https://doi.org/10.1116/1.569075.

[28] G.L. Harding, S. Craig, Magnetron-sputtered metal carbide solar selective absorbing surfaces, J. Vac. Sci. Technol. 16 (1979) 857–862, https://doi.org/10.1116/1.570100.

[29] A. Mourlas, E. Pavlidou, G. Vourlias, J. Rodríguez, P. Psyllaki, Concentrated solar energy for in-situ elaboration of wear-resistant composite layers. Part I: TiC and chromium carbide surface enrichment of common steels, Surf. Coat. Technol. 377 (2019), 124882, https://doi.org/10.1016/j.surfcoat.2019.08.011.

[30] V. Sreenivasulu, M. Manikandan, High-temperature corrosion behaviour of air plasma sprayed Cr3C2-25NiCr and NiCrMoNb powder coating on alloy 80A at 900°C, Surf. Coat. Technol. 337 (2018) 250–259, https://doi.org/10.1016/j.surfcoat.2018.01.011.

[31] DSMTS-0027.5, Woka 7100 CrC-NiCr Series, 2014.

[32] D.C, Montgomery, Design and Analysis of Experiments, Ninth, John Wiley & Sons, Inc, Hoboken, NJ, 2017.

[33] ASTM International, ASTM D 4541-17 standard test method for pull-off strength of coatings using portable adhesion testers, in: Book of Standards, West Conshohocken, PA, USA, 2017.

[34] L. Venkatesh, S.B. Pitchuka, G. Sivakumar, R.C. Gundakaram, S.V. Joshi, I. Samajdar, Microstructural response of various chromium carbide based coatings to erosion and nano impact testing, Wear 386–387 (2017) 72–79, https://doi.org/10.1016/J.WEAR.2017.06.002.

[35] G.-C. Ji, C.-J. Li, Y.-Y. Wang, W.-Y. Li, Microstructural characterization and abrasive wear performance of HVOF sprayed Cr3C2–NiCr coating, Surf. Coat. Technol. 200 (2006) 6749–6757, https://doi.org/10.1016/j.surfcoat.2005.10.005.

[36] L. Venkatesh, I. Samajdar, M. Tak, R.D. Doherty, R.C. Gundakaram, K.S. Prasad, S. V. Joshi, Microstructure and phase evolution in laser clad chromium carbide-NiCrMoNb, Appl. Surf. Sci. 357 (2015) 2391–2401, https://doi.org/10.1016/j.apsusc.2015.09.260.

[37] M. Venkatraman, J.P. Neumann, The C-cr (Carbon-Chromium) system, Bull. Alloy Phase Diagr. 11 (1990) 152–159, https://doi.org/10.1007/BF02841701.

[38] D.-Y. Kim, M.S. Han, J.-G. Youn, Characterization of erosion resistant Cr3C2-NiCr plasma sprayed coatings, in: C.C. Berndt (Ed.), Thermal Spray: Practical Solutions for Engineering Problems: Proceedings of the 9th National Thermal Spray Conference, ASM International, Materials Park, Ohio-USA, Cincinnati (OH), 1996, pp. 123–128.